

# Thio-oxynitride phosphate glass electrolytes prepared by mechanical milling

Nerea Mascaraque<sup>a)</sup>

Glasses Department, Instituto de Cerámica y Vidrio (CSIC), Cantoblanco, Madrid 28049, Spain

José Luis G. Fierro

Group of Sustainable Energy and Chemistry, Instituto de Catálisis y Petroquímica (CSIC), Cantoblanco, Madrid 28049, Spain

Francisco Muñoz and Alicia Durán

Glasses Department, Instituto de Cerámica y Vidrio (CSIC), Cantoblanco, Madrid 28049, Spain

Yusuke Ito, Yoshiaki Hibi, Ryo Harada, Atsutaka Kato, Akitoshi Hayashi, and Masahiro Tatsumisago

Department of Applied Chemistry, Graduate School of Engineering, Osaka Prefecture University, Sakai, Osaka 599-8531, Japan

(Received 11 February 2015; accepted 21 April 2015)

Lithium thio-phosphorus oxynitride glasses, LiPOSN, have been prepared by mechanical milling process from the mixture of  $\text{Li}_2\text{S}$  and LiPON glass. The anionic substitution of oxygen by sulphur and nitrogen in the phosphate glass structure has been confirmed by  $1\text{D } ^{31}\text{P}$  solid state nuclear magnetic resonance and x-ray photoelectron spectroscopy. The study of thermal and electrical properties reveals a decrease in the glass transition temperature, likely due to the depolymerization of glass network by the decrease of bridging oxygens and sulphurs, along with a sharp increase in the ionic conductivity when lithium sulphide is incorporated into the oxynitride glasses. The improvement of chemical durability by the introduction of nitrogen, together with the increase in ionic conductivity up to values closed to the value of commercial LiPON thin film electrolyte, suggests that these LiPOSN glasses could be good candidates as solid electrolytes for lithium microbatteries.

## I. INTRODUCTION

In the last few decades, solid electrolytes have gained much interest due to their application in lithium batteries. In particular, sulphide glasses, which are materials with the highest ionic conductivity and better performance, have been reported by many authors, as thin films,<sup>1–5</sup> powders,<sup>6–10</sup> and glass-ceramics.<sup>11,12</sup> In general, these studies are based on the preparation of  $\text{Li}_2\text{S}-\text{P}_2\text{S}_5$  materials, where  $\text{GeS}_2$ ,  $\text{GeSe}_2$ ,  $\text{Ga}_2\text{S}_3$  or  $\text{SiS}_2$  is introduced to obtain high values of ionic conductivity ( $<10^{-4}$  S/cm). However, the main disadvantage of the materials with  $\text{Li}_2\text{S}$  is the low chemical durability that produces a high degradation in air, being necessary the manipulation of these materials in an inert atmosphere. Minami et al. and Ohtomo et al.<sup>13,14</sup> demonstrated that the introduction of 3 mol%  $\text{P}_2\text{O}_5$  and 17–25 mol%  $\text{Li}_2\text{O}$ , respectively, in the system of  $\text{Li}_2\text{S}-\text{P}_2\text{S}_5$  produces an increase in the ionic conductivity and chemical stability.

On the other hand, in pure oxide glasses, such as the  $\text{Li}_2\text{O}-\text{P}_2\text{O}_5$  system,<sup>15–19</sup> oxygen substitution by nitrogen

leads to an increase of nonbridging oxygens (NBO) contents, along with an increase in the connectivity of the glass network by the formation of P–N bonds, which have higher covalent character than P–O bonds. These structural changes can explain the increase in the thermal and chemical stability, together with the ionic conductivity. Besides, the increase of ionic conductivity by the effect of nitrogen also depends on the addition of lithium content, as observed by Mascaraque et al.<sup>19</sup> Thus, it is expected that the introduction of lithium sulphide in nitrided phosphate glasses results in a simultaneous improvement of electrical and chemical properties that allows their application as solid electrolytes.

Nowadays, the study on  $\text{Li}_2\text{S}-\text{P}_2\text{S}_5$  glasses has been basically focused on electrical and electrochemical properties, without emphasizing their structure. In a preliminary study on  $\text{Li}_2\text{O}-\text{Li}_2\text{S}-\text{P}_2\text{O}_5-\text{PON}$  glass prepared for the first time by melting,<sup>20</sup> it has been demonstrated that the introduction of  $\text{Li}_2\text{S}$  and nitrogen produces a notable increase in the ionic conductivity. This process consists of two-step melting from the mixture of  $\text{Li}_2\text{S}$  and LiPON glass, which was previously obtained by ammonolysis.<sup>18,21</sup>

In this work, mechanical milling (MM) was used for the preparation of LiPOSN glasses from the starting

Contributing Editor: Zoltan Lences

<sup>a)</sup>Address all correspondence to this author.

e-mail: mascaraque@icv.csic.es

DOI: 10.1557/jmr.2015.128

materials, Li<sub>2</sub>S and LiPON glasses, to arrive to final composition and a comparison between both procedures was performed. The main objectives are to increase the ionic conductivity with the simultaneous enhancement of chemical durability and to study the structure of the materials in detail. The structure of LiPOSN materials was performed through nuclear magnetic resonance (NMR) and x-ray photoelectron spectroscopy (XPS), and their electrical and thermal properties were studied through electrochemical impedance spectroscopy and differential scanning calorimetry (DSC).

## II. EXPERIMENTAL

### A. Preparation of LiPON glass

A parent glass of 55Li<sub>2</sub>O·45P<sub>2</sub>O<sub>5</sub>, which has already been studied in Ref. 19, was firstly prepared by melt-quenching from batches of reagent grade materials such as Li<sub>2</sub>CO<sub>3</sub> (99% ACS Reagent, Aldrich) and (NH<sub>4</sub>)<sub>2</sub>HPO<sub>4</sub> (99% ACS Reagent, Merck). The batch was calcined in a porcelain crucible in an electric furnace up to 400 °C for 1 day and melted for 2 h at 850 °C. The glass was obtained by pouring the melt onto a brass plate. Finally, the glass was nitrided following a thermal treatment under anhydrous ammonia at 750 °C for 5 h, obtaining the glass called as 55LiPON.

### B. Preparation of LiPOSN samples

The powdered materials belonging to Li<sub>2</sub>S-LiPON system were prepared from 1 g batches of reagent grade Li<sub>2</sub>S (99.9%) and LiPON glass by MM using a planetary ball mill (Fritsch Pulverisette 7) introduced in a glove box with Ar gas, with a ZrO<sub>2</sub> pot (volume, 45 cm<sup>3</sup>) with 500 ZrO<sub>2</sub> balls (diameter, 4 mm). The spinning rate was 510 rpm with milling time between 7 and 20 h, depending on the composition.

### C. Characterization of the glasses

X-ray powder diffraction (XRD) patterns were obtained in a diffractometer (Rigaku, Ultima IV) using monochromatic Cu K<sub>α</sub> radiation ( $\lambda = 1.540598$ ). Scan rate is 2° per minute at 2θ from 10° to 60°. The total measuring time is 25 min.

The weight percentages of nitrogen and sulphur in powdered samples were determined using an analyzer LECO CHNS-932 (LECO corporation, St. Joseph, MI), verifying the simultaneous existence of nitrogen and sulphur in the phosphate network. The errors of nitrogen and sulphur analyses are ±0.3 and ±0.2 mol%, respectively.

<sup>31</sup>P magic angle spinning (MAS)-nuclear magnetic resonance (NMR) experiments were performed on a 9.4 T Bruker spectrometer at 162.9 MHz. The 1D MAS-NMR spectra were conducted at a spinning frequency of 15 kHz with a 4 mm probe-head. The experiments were recorded with a 4 μs pulse length

(π/2 pulse angle), a radiofrequency (rf) strength of 60 kHz, and 128 transients separated by a recycle delay (rd) of 60 s.

Photoelectron spectra (XPS) were obtained with a VG Escalab 200R spectrometer equipped with a MgK<sub>α</sub> ( $h\nu = 1253.6$  eV, 1 eV =  $1.6302 \times 10^{-19}$  J) x-ray source, powered at 120 W. The XPS data signals were taken in increments of 0.07 eV with a dwell time of 50 ms. Binding energies were calibrated relative to the C<sub>1s</sub> peak at 284.8 eV. Atomic ratios were computed from experimental intensity ratios and normalized by atomic sensitivity factors.<sup>22</sup>

The glass transition temperature,  $T_g$ , was determined by DSC in a Discovery DSC (TA Instruments), which employs a constant heating rate of 10 °C/min under argon flow and between 25 and 500 °C. The  $T_g$  error is within ±5 °C.

A JSM-6610A (JEOL Ltd., Tokyo, Japan) scanning electron microscope was used to determine the thickness of the LiPOSN materials. This equipment is equipped with an energy dispersive x-ray spectroscopy system (JED-2300, JEOL Ltd., Tokyo, Japan).

Ionic conductivity measurements were conducted under dry Ar atmosphere using a SI-1260 impedance analyzer from Solartron, in the frequency range from 0.1 to 1 MHz and a voltage of 50 mV. The LiPOSN powder (100 mg) was pressed at 360 MPa for 1 min to form a pellet, and foils were placed on both the surfaces of the pellet, followed by pressing at 100 MPa. Stainless steel disks were attached to the pellet as current collectors. The diameter of the pellets was 10 mm and the thickness was 0.33–1.14 mm. The AC impedance measurements were performed at 25 °C for the amorphous samples. The conductivity ( $\sigma$ ) is calculated using the equation:

$$\sigma = (1/R) \cdot (d/S) , \quad (1)$$

being  $(d/S)$  the sample geometric factor, where  $d$  is thickness and  $S$  is sample area.

## III. RESULTS AND DISCUSSION

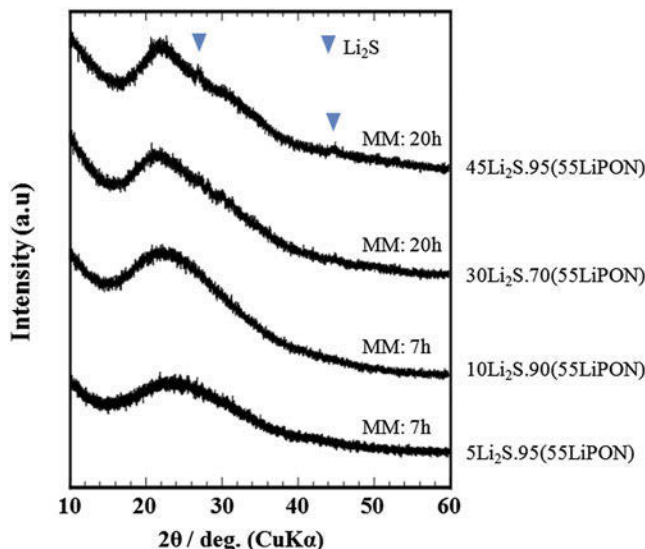
### A. Composition of samples

Table I shows the molar percentage of nominal and analyzed sulphur and nitrogen contents of the samples  $x\text{Li}_2\text{S} \cdot (100 - x) \text{ (55Li}_2\text{O}\cdot\text{45P}_2\text{O}_5 + \text{N})$  with Li<sub>2</sub>S contents between 5 and 95 mol%. The loss of sulphur is very low, just 2–10% in milled powders, but nitrogen losses increase with increasing Li<sub>2</sub>S contents, from 0% for samples with 5 and 10 mol% Li<sub>2</sub>S to 30–40% for samples with 30 and 45 mol% Li<sub>2</sub>S. The milled powders with 90 and 95 mol% Li<sub>2</sub>S were not characterised because the samples were not amorphous after 80 h of milling, likely due to the excess of Li<sub>2</sub>S content.

Figure 1 represents the XRD patterns of LiPOSN samples with 5–45 mol% Li<sub>2</sub>S. In the range of composition between 5 and 30 mol% Li<sub>2</sub>S, the samples are amorphous, but in the case of the sample with 45 mol%

TABLE I. Molar percentage of lithium, sulphur, and nitrogen of the samples  $x\text{Li}_2\text{S}(100 - x)(55\text{Li}_2\text{O}\cdot45\text{P}_2\text{O}_5 + \text{N})$  ( $x = 5\text{--}95\text{ mol\%}$ ).

Samples	%Li <sub>nominal</sub>	%N <sub>nominal</sub>	%N <sub>analyzed</sub> ( $\pm 0.3\%$ )	N <sub>anal./N<sub>nom.</sub></sub>	%S <sub>nominal</sub>	%S <sub>analyzed</sub> ( $\pm 0.2\%$ )	S <sub>anal./S<sub>nom.</sub></sub>
55LiPON	22.9	...	6.6	...	...	...	...
5Li <sub>2</sub> S-95(55LiPON)	24.3	6.6	6.6	1.00	1.1	1.0	0.91
10Li <sub>2</sub> S-90(55LiPON)	25.5	6.6	6.6	1.00	2.2	2.1	0.95
30Li <sub>2</sub> S-70(55LiPON)	32.2	6.6	4.4	0.69	7.0	6.8	0.97
45Li <sub>2</sub> S-55(55LiPON)	37.7	6.6	4.0	0.61	11.3	11.1	0.98
90Li <sub>2</sub> S-10(55LiPON)	60.1	6.6	...	...	28.3	...	...
95Li <sub>2</sub> S-5(55LiPON)	63.3	6.6	...	...	30.7	...	...

FIG. 1. X-ray diffractogram patterns of samples  $x\text{Li}_2\text{S}(100 - x)(55\text{Li}_2\text{O}\cdot45\text{P}_2\text{O}_5 + \text{N})$  ( $x = 5\text{--}45\text{ mol\%}$ ) prepared by MM for time periods of 7 and 20 h.

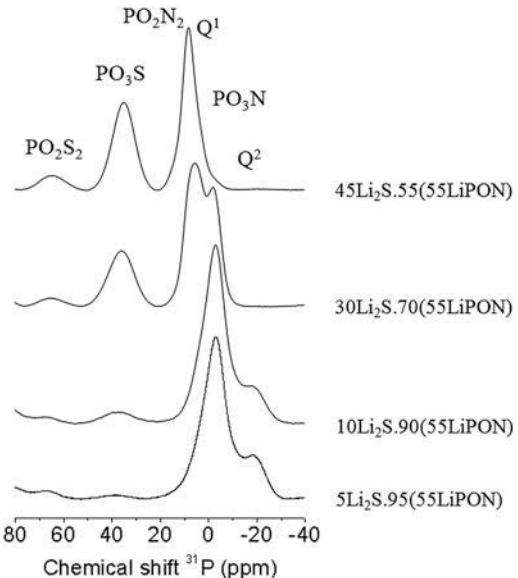
$\text{Li}_2\text{S}$ , peaks with very low intensity appear and correspond to a crystalline phase of  $\text{Li}_2\text{S}$ , indicating that this composition is the limit of  $\text{Li}_2\text{S}$  content, which can be introduced in lithium phosphorus oxynitride glasses.

## B. Structure

The structure of all the LiPOSN samples was studied through  $^{31}\text{P}$  MAS NMR and XPS. Through NMR, the phosphorus groups with and without nitrogen and sulphur can be identified. XPS of  $\text{N}_{1s}$ ,  $\text{O}_{1s}$ , and  $\text{S}_{2p}$  allows determination of the ratio BO/NBO (bridging oxygens/NBO),  $N_t/N_d$  (nitrogen tri-coordinated/nitrogen di-coordinated), and BS/NBS (bridging sulphurs/non-bridging sulphurs).

### 1. $^{31}\text{P}$ MAS NMR

Figure 2 gathers that the  $^{31}\text{P}$  MAS NMR spectra of powdered glasses obtained by MM reveal two broad resonance bands in the range of 20 and  $-25\text{ ppm}$  and two resonances comprised between 70 and  $30\text{ ppm}$ . According to the literature,<sup>6,23–25</sup> the resonances appearing at

FIG. 2.  $^{31}\text{P}$  MAS NMR spectra of powdered lithium thio-phosphorus oxynitride samples.

35 and  $65\text{ ppm}$  may be assigned to  $\text{PO}_2\text{S}_2$  and  $\text{PO}_3\text{S}$  units. For contents of lithium sulphide up to  $10\text{ mol\%}$ , the two broad resonances which maxima at  $-19$  and  $2\text{ ppm}$  may correspond to  $\text{Q}^2$  and  $\text{Q}^1$  groups.<sup>26</sup> These samples present nitrogen, so  $\text{PO}_3\text{N}$  and  $\text{PO}_2\text{N}_2$ <sup>27,28</sup> groups are expected to appear at  $-11$  and  $6\text{ ppm}$ , likely overlapped with other broad resonances. For higher  $\text{Li}_2\text{S}$  contents ( $30$  and  $45\text{ mol\%}$ ), the band assigned to  $\text{Q}^2$  groups disappears, indicating that the sulphur and lithium introduction produces the decrease of P–O–P bonds to form phosphate groups with one or two sulphurs,  $\text{PO}_3\text{S}$  or  $\text{PO}_2\text{S}_2$  species. The broad band situated between  $6$  and  $-11\text{ ppm}$  could correspond to several overlapping resonances assigned to  $\text{Q}^1$  groups at  $2\text{ ppm}$ ,<sup>26</sup> and phosphorus species with nitrogen,  $\text{PO}_2\text{N}_2$ , and  $\text{PO}_3\text{N}$ , at  $-11$  and  $6\text{ ppm}$ .<sup>27,28</sup>

### 2. XPS of $\text{N}_{1s}$ peak

Figure 3 represents XPS spectra of the  $\text{N}_{1s}$  peak of all lithium thio-phosphorus oxynitride samples. The spectra are deconvoluted into two Gaussian–Lorentzian mixed components assigned to two different bonding states of

nitrogen atoms.<sup>17,29–31</sup> The first component corresponds to nitrogen 2-fold coordinated ( $N_d$ ) at  $\sim 398.2$  eV, and second one to nitrogen 3-fold coordinated ( $N_t$ ) at  $\sim 399.5$  eV.

From the deconvolution of XPS spectra of  $N_{1s}$ , the values of  $N_t/N_d$  can be calculated and are collected in Table II. The nitrogen content of the samples with 5 and 10 mol%  $\text{Li}_2\text{S}$  does not change respecting to base oxynitride glass (Table I), so similar values of  $N_t/N_d$  are expected. However, glasses with 30 and 45 mol%  $\text{Li}_2\text{S}$  present lower nitrogen contents. Following the study of  $N_{1s}$  XPS of lithium phosphorus oxynitride glasses,<sup>19</sup> the lower the nitrogen content, the higher will be the  $N_t/N_d$  ratio.

### 3. XPS of $O_{1s}$ peak

Figure 4 shows the XPS spectra of the  $O_{1s}$  peak of all powdered samples. The spectra are deconvoluted into

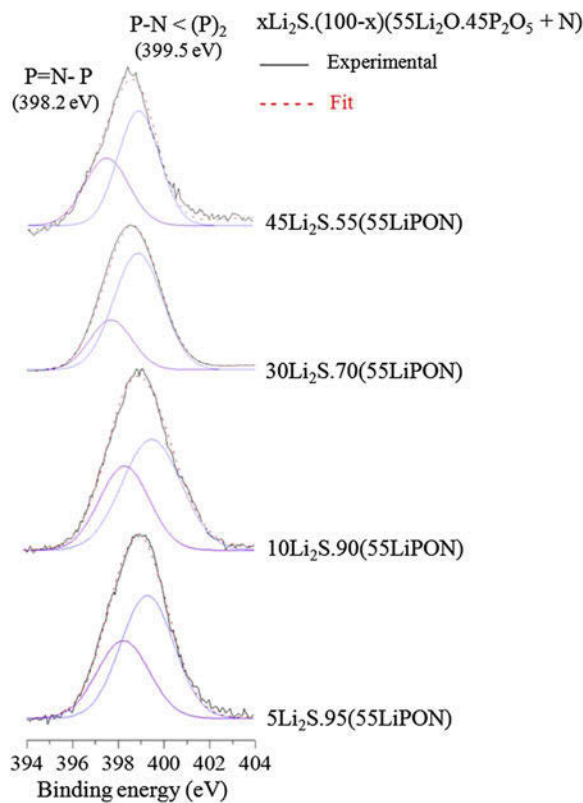


FIG. 3. XPS spectra of the  $N_{1s}$  peak of samples  $x\text{Li}_2\text{S}(100 - x)$  ( $55\text{Li}_2\text{O}\cdot45\text{P}_2\text{O}_5 + \text{N}$ ), where  $x = 5, 10, 30$ , and  $45$  mol%.

TABLE II.  $N_t/N_d$ , BO/NBO, and BS/NBS ratios of LiPOSN samples, with an error of  $\pm 0.05$ .

Samples	$N_t/N_d$ ratio	BO/NBO ratio	BS/NBS ratio
55LiPON	1.76	...	...
5Li <sub>2</sub> S-95(55LiPON)	1.62	0.35	0.64
10Li <sub>2</sub> S-90(55LiPON)	1.57	0.27	0.43
30Li <sub>2</sub> S-70(55LiPON)	2.57	0.18	0.24
45Li <sub>2</sub> S-55(55LiPON)	2.45	0.09	0.09

three Gaussian–Lorentzian mixed components attributed to two types of NBO,  $\text{P}=\text{O}$  at  $\sim 530.7$  eV and  $\text{Li}^+ \dots \text{O}-\text{P}$  at  $\sim 531.6$  eV, and another component to BO at  $\sim 533.5$  eV.<sup>32</sup> From the deconvolution of XPS spectra of  $O_{1s}$  peaks, the BO/NBO ratio can be calculated as a function of sulphur content introduced in lithium phosphorus oxynitride glasses, Table II. The increase of lithium sulphide content in phosphate glasses produces the decrease of BO, related to the breaking of phosphate chains produced by the introduction of lithium, as observed by Mascaraque et al.,<sup>20</sup> and/or the substitution of BO and NBO by sulphur.

### 4. XPS of $S_{2p}$ peak

Figure 5 presents the spectra of the  $S_{2p}$  peak of powder LiPOSN amorphous materials. These spectra are deconvoluted into two components assigned to NBS at  $\sim 162.0$  eV and BS at  $\sim 163.8$  eV. In this case, the spectra can only be deconvoluted into two components due to low sensibility of XPS equipment for lower bonding energy; although, this type of spectrum of  $S_{2p}$  peak should be deconvoluted into four Gaussian–Lorentzian mixed components.<sup>33</sup> In Table II, the ratio of BS/NBS obtained from the deconvolution of XPS spectra of  $S_{2p}$  is indicated, as a function of sulphur content in lithium phosphorus oxynitride glasses. Oxygen is substituted by

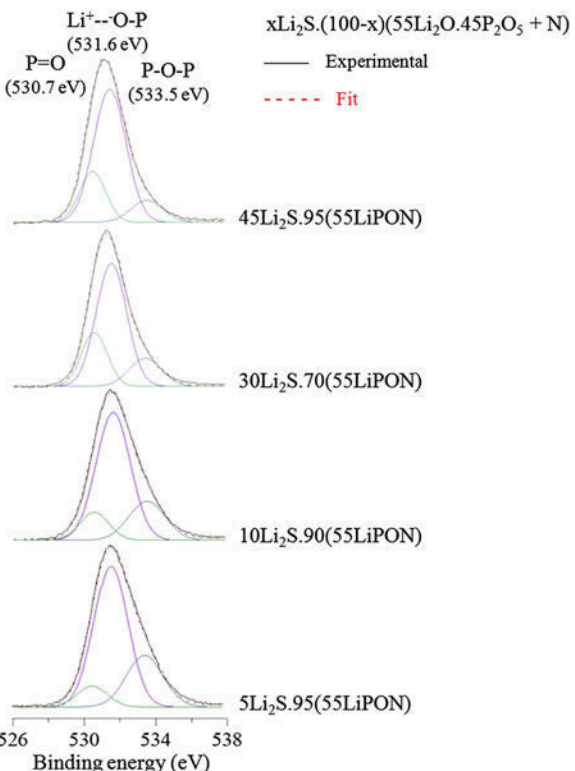


FIG. 4. XPS spectra of the  $O_{1s}$  peak of samples  $x\text{Li}_2\text{S}(100 - x)$  ( $55\text{Li}_2\text{O}\cdot45\text{P}_2\text{O}_5 + \text{N}$ ), where  $x = 5, 10, 30$ , and  $45$  mol%.

sulphur in the phosphate glasses to lead to BS and NBS. The increase of  $\text{Li}_2\text{S}$  content produces an increase of NBS.

## 5. Structural interpretation

The structural interpretation is derived from the information obtained by NMR and XPS techniques:

(i) The increase of molar percentage of  $\text{Li}_2\text{S}$  leads to the decrease of BO/NBO and BS/NBS ratios (Table II). For the sample with 45 mol%  $\text{Li}_2\text{S}$ , the percentage of BO and BS is just 10% of their total contents.

(ii) The introduction of lithium and sulphur produces the decrease of P–O–P bonds by the formation of phosphate groups,  $\text{Q}^2$  and  $\text{Q}^1$ , with sulphurs,  $\text{PO}_3\text{S}$ , and  $\text{PO}_2\text{S}_2$  species. For higher  $\text{Li}_2\text{S}$  contents (30 and 45 mol%), the  $\text{Q}^2$  groups disappear (Fig. 2).

(iii) The percentages of  $\text{PO}_3\text{S}$  and  $\text{PO}_2\text{S}_2$  species increase with increasing lithium sulphide content, in particular, for samples with  $\text{Li}_2\text{S}$  contents higher than 30 mol%.

(iv)  $5\text{Li}_2\text{S}\cdot95(55\text{LiPON})$  and  $10\text{Li}_2\text{S}\cdot90(55\text{LiPON})$  samples present a  $N/N_d$  ratio of approximately 1.6, while  $30\text{Li}_2\text{S}\cdot70(55\text{LiPON})$  and for  $45\text{Li}_2\text{S}\cdot55(55\text{LiPON})$  samples, which present lower amount of nitrogen, the  $N/N_d$  ratio is of approximately 2.5.

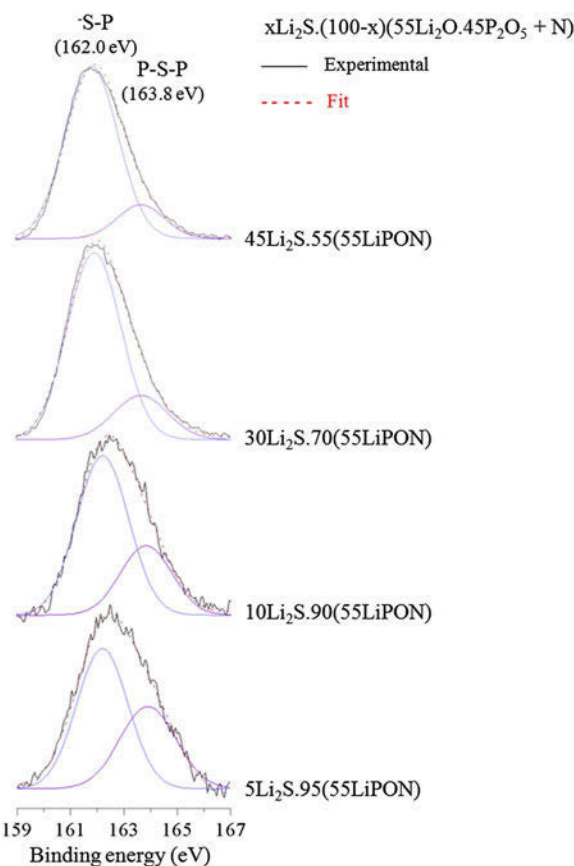


FIG. 5. XPS spectra of the  $\text{S}_{2p}$  peak of samples  $x\text{Li}_2\text{S}(100 - x)$  ( $55\text{Li}_2\text{O}\cdot45\text{P}_2\text{O}_5 + \text{N}$ ), where  $x = 5, 10, 30$ , and  $45$  mol%.

The structure of  $5\text{Li}_2\text{S}\cdot95(55\text{LiPON})$  and  $10\text{Li}_2\text{S}\cdot90$  ( $55\text{LiPON}$ ) materials may be thought to be similar to that of a conventional glass structure. However, in the  $30\text{Li}_2\text{S}\cdot70(55\text{LiPON})$  and  $45\text{Li}_2\text{S}\cdot55(55\text{LiPON})$  samples, there are an 80–90% of BO and BS, a lack of  $\text{Q}^2$  groups, and a significant percentage of  $\text{PO}_3\text{S}$  and  $\text{PO}_2\text{S}_2$  units. These results suggest that these materials present an ionic structure with isolated species and regions with phosphate groups with and without sulphur and connected through P–N bonds of the  $\text{PO}_3\text{N}$  and  $\text{PO}_2\text{N}_2$  species.

## C. Properties

### 1. Thermal properties

Figure 6 shows the DSC patterns of all powdered samples. Glass transition temperature obtained through DSC curves decreases after incorporation of S into the oxynitride glass down to  $50^\circ\text{C}$  less for the 45 mol%  $\text{Li}_2\text{S}$  sample due to the formation of  $\text{PO}_3\text{S}$  species with lower number of BO-atoms and the presence of NBS-atoms, as observed by XPS (Figs. 4 and 5 and Table II). Besides, the materials with 5 and 10 mol%  $\text{Li}_2\text{S}$  present an exothermal peak at  $270^\circ\text{C}$  (denoted with red star), which can be due to a crystallization peak.

### 2. Ionic conductivity

Figure 7 represents Nyquist diagrams at room temperature of all studied samples. Applying Eq. (1), the values of ionic conductivity at room temperature were calculated

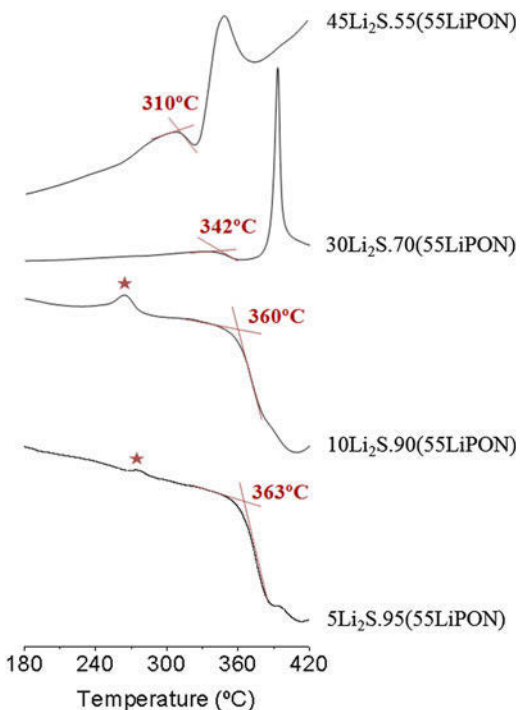


FIG. 6. DSC curves of samples  $x\text{Li}_2\text{S}(100 - x)$   $55\text{Li}_2\text{O}\cdot45\text{P}_2\text{O}_5 + \text{N}$ , where  $x = 5, 10, 30$ , and  $45$  mol%.

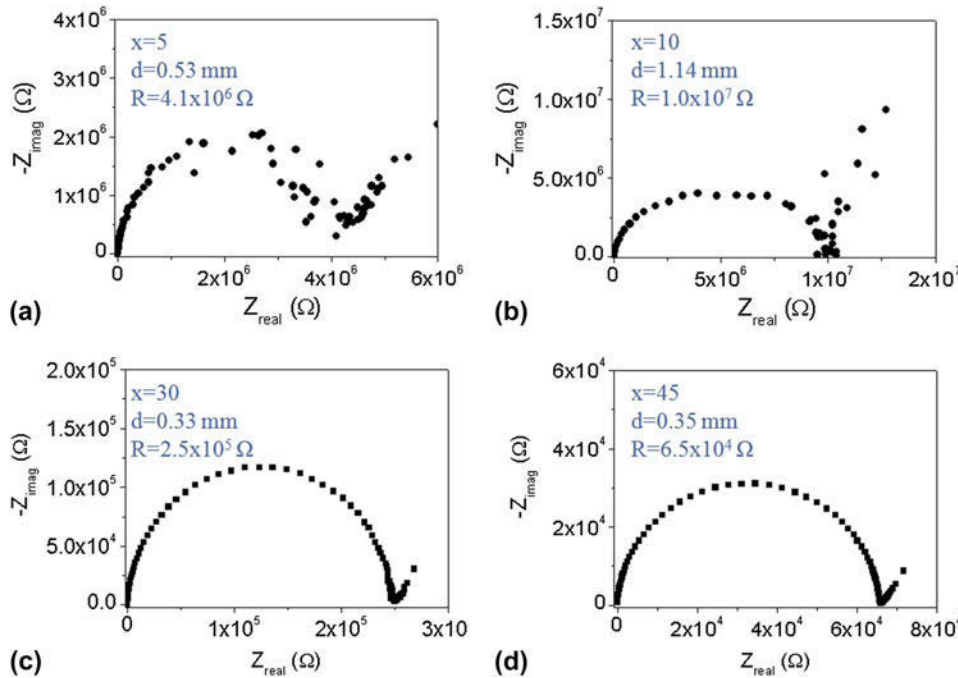


FIG. 7. Nyquist diagrams at room temperature of powder samples  $x\text{Li}_2\text{S}(100 - x)\text{55Li}_2\text{O}\cdot\text{45P}_2\text{O}_5 + \text{nitrógeno}$ , where  $x$  is (a) 5, (b) 10, (c) 30, and (d) 45 mol%.

and are presented in Table III. The values of  $\sigma$  indicate that the introduction of lithium sulphide in lithium phosphorus oxynitride glasses produces a significant increase in their conductivity, with a difference of nearly two orders of magnitude between glasses with 5 and 45% mol% Li<sub>2</sub>S (Table III). On the other hand, it should be noted that the precursor 55LiPON is a bulk glass obtained by melting, while glasses with Li<sub>2</sub>S are compressed powder pellets, so, it is expected that the pellet with the lowest Li<sub>2</sub>S presents lower ionic conductivity compared to bulk 55LiPON glass.

The pellets of powdered materials present ionic conductivity of the grain boundaries and within the grains. The resistance of grain boundaries is very high compared to the grain, decreasing the total ionic conductivity of the sample. To monitor and minimize the effect of grain boundaries, glasses with 5 and 10 mol% Li<sub>2</sub>S were selected to be pressed for 5 h at 360 °C [corresponding to glass transition temperature (Fig. 8)], and the sample with 10 mol% Li<sub>2</sub>S was also pressed at lower temperature, 270 °C, for 5 h to observe the effect of the pressing temperature on ionic conductivity.

Figure 8 shows the Nyquist diagrams of the pellets obtained by hot-pressing, from which the resistances at room temperature are obtained, and applying Eq. (1), the values of ionic conductivity at 25 °C are calculated and gathered in Table III. The ionic conductivity values indicate that both treatments allow reducing the effect of grain boundary, the total log ionic conductivity increases up to -7.46 and -6.99 ( $\sigma$  in S/cm) in the glasses with 5 and 10 mol% Li<sub>2</sub>S, respectively. However, the temperature used

TABLE III. Ionic conductivity at room temperature of all pellets obtained by cold-pressing, and the pellets with 5 and 10 mol% Li<sub>2</sub>S prepared by hot-pressing (270 and 360 °C).

Samples	Pressed temperature (°C)	$\log \sigma_{25} \text{ °C}$ ( $\sigma$ in S/cm)
55LiPON	...	-7.80
5Li <sub>2</sub> S-95(55LiPON)	25	-7.99
	360	-7.46
	25	-7.84
10Li <sub>2</sub> S-90(55LiPON)	270	-7.21
	360	-6.99
30Li <sub>2</sub> S-70(55LiPON)	25	-6.77
45Li <sub>2</sub> S-55(55LiPON)	25	-6.17

has a strong influence on the ionic conductivity. Indeed, the pellet with 10 mol% Li<sub>2</sub>S pressed at 270 °C has a lower conductivity with respect to that pressed at 360 °C. Images of scanning electron microscopy (SEM) show that samples pressed at 360 °C are dense [Figs. 9(a) and 9(c)], with a small porosity on the sample with 5 mol% Li<sub>2</sub>S that could explain the lower increase in conductivity with respect to 10Li<sub>2</sub>S-90(55LiPON). The pellet with 10 mol% Li<sub>2</sub>S pressed at 270 °C shows a high porosity [Fig. 9(b)] and is only dense when pressed at 360 °C, where higher ionic conductivity is obtained.

#### D. Relationship between ionic conductivity and structure

The XPS spectra of O<sub>1s</sub> and S<sub>2p</sub> peaks permit to calculate the percentage of BO and NBO and sulphurs, which is related to the electrical properties. Figure 10 indicates that

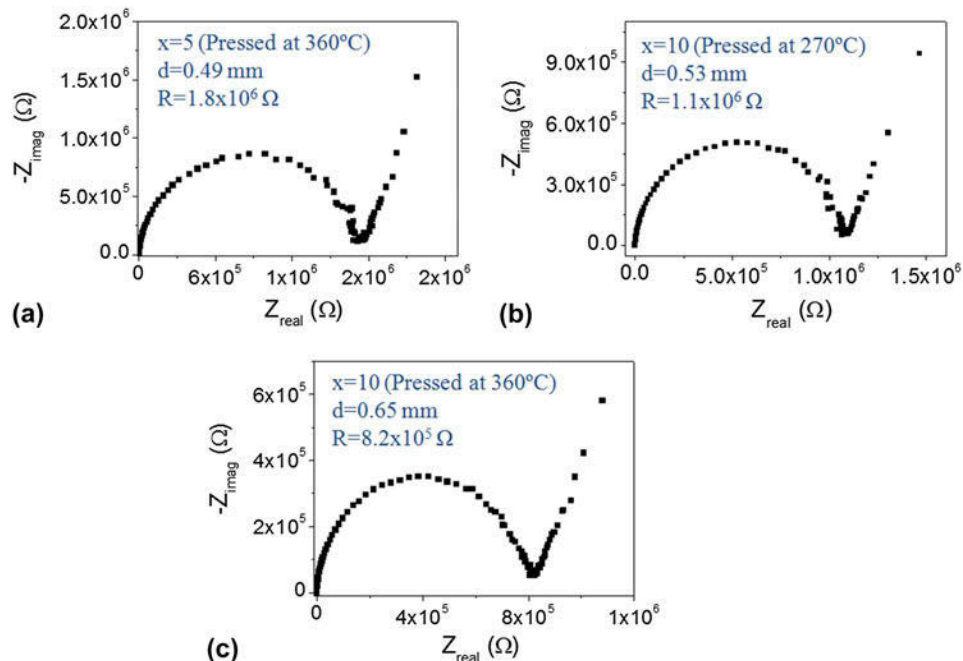


FIG. 8. Nyquist diagrams at room temperature of amorphous materials with 5 mol% Li<sub>2</sub>S pressed at (a) 360 °C, with 10 mol% Li<sub>2</sub>S pressed at (b) 270 °C and (c) 360 °C.

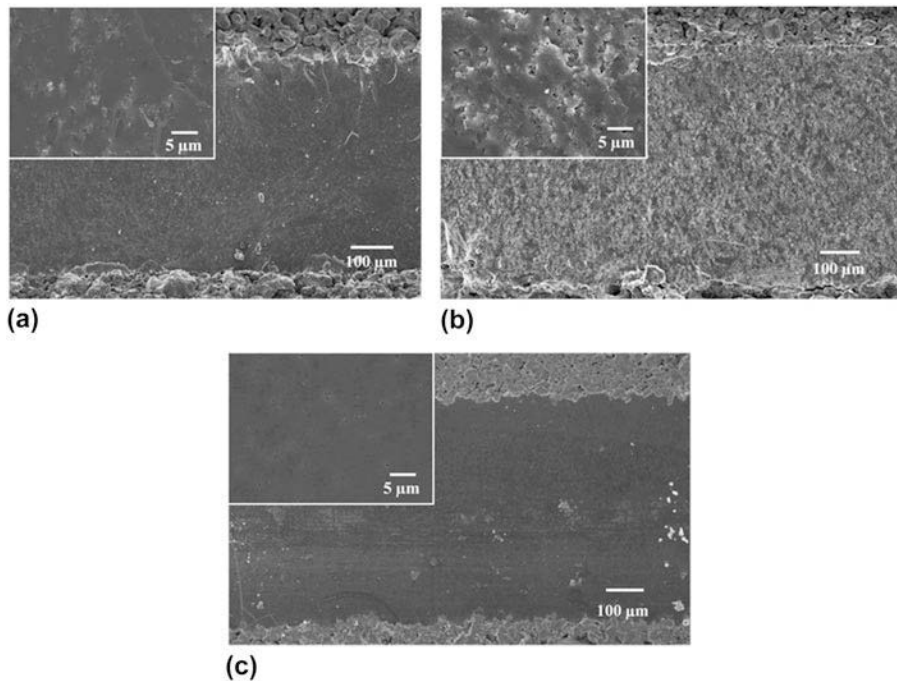


FIG. 9. SEM images of pellets with 5 mol% Li<sub>2</sub>S pressed at (a) 360 °C, with 10 mol% Li<sub>2</sub>S pressed at (b) 270 °C and (c) 360 °C.

the higher the decrease of BO/NBO and BS/NBS ratios and the higher the increase of ionic conductivity. The introduction of lithium sulphide leads to the breaking of phosphate chains by the double effect of lithium, a network modifier, and the substitution of BO by sulphur. Both effects produce the decrease of BO/NBO ratio, directly related to the increase of ionic conductivity. Besides, the

introduction of 5 mol% Li<sub>2</sub>S (1 mol% S) leads to the formation of BS and NBS, having a 61% of NBS. With increasing Li<sub>2</sub>S content, the proportion of NBS gives rise up to 92%. The sharp decrease of BS/NBS appears as a direct cause of increased ionic conductivity, which is of nearly two orders of magnitude with respect to the glass with the lowest sulphur content.

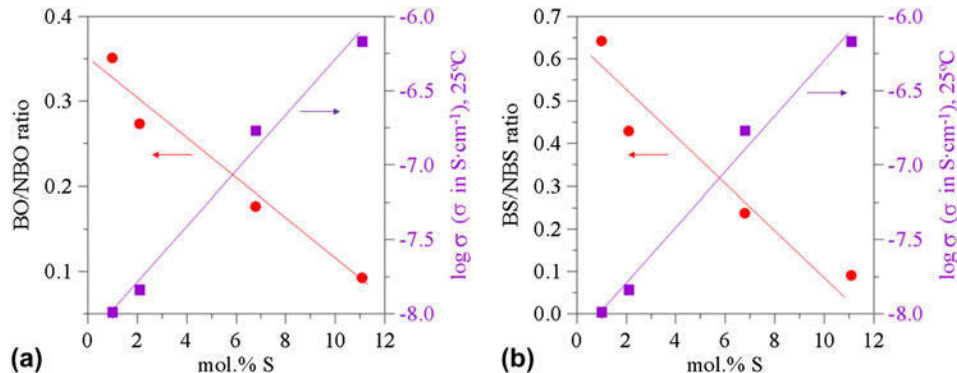


FIG. 10. Log  $\sigma$  at room temperature and (a) BO/NBO or (b) BS/NBS ratios, as a function of sulphur content of LiPOSN samples.

In samples with 30 and 45 mol% Li<sub>2</sub>S, which present the highest ionic conductivities, the results of NMR indicate the presence of ionic structures with isolated groups and low ratios of BO/NBO and BS/NBS that could improve the mobility of Li<sup>+</sup> ions, leading to an increase of conductivity.

#### IV. CONCLUSIONS

The MM process starting from an oxynitride glass and Li<sub>2</sub>S allowed preparation of high lithium phosphate glasses containing both S- and N-anions. NMR and XPS demonstrated that both N and S substitute for the anionic positions in the Li-phosphate glasses. The structural results suggest that powder glasses with high sulphur content present an ionic type structure with isolated species and regions with PO<sub>4</sub>, PO<sub>3</sub>S, and PO<sub>2</sub>S<sub>2</sub> groups, only connect through the PO<sub>3</sub>N and PO<sub>2</sub>N<sub>2</sub> units. The double substitution of oxygen by nitrogen and sulphur in lithium phosphate glasses leads to a significant increase in the ionic conductivity. The enhancement of conductivity is related to the structural changes, being that the higher decrease of ratios of BO and NBO and sulphurs leads to the higher mobility of Li<sup>+</sup> ions, i.e., the higher increase of ionic conductivity.

#### ACKNOWLEDGMENTS

Financial support from project MAT2010-20459 is greatly acknowledged. N. Mascaraque thanks MEC ministry for funding of a FPU-2009 grant. María José de la Mata (SIDI-UAM) is also greatly acknowledged for her assistance in the NMR characterization.

#### REFERENCES

- Y. Ito, A. Sakuda, T. Ohtomo, A. Hayashi, and M. Tatsumisago: Preparation of Li<sub>2</sub>S–GeS<sub>2</sub> solid electrolyte thin films using pulsed laser deposition. *Solid State Ionics* **236**, 1 (2013).
- A. Sakuda, A. Hayashi, T. Ohtomo, S. Hama, and M. Tatsumisago: All-solid-state lithium secondary batteries using LiCoO<sub>2</sub> particles with pulsed laser deposition coatings of Li<sub>2</sub>S–P<sub>2</sub>S<sub>5</sub> solid electrolytes. *J. Power Sources* **196**, 6735 (2011).
- Y. Sakurai, A. Sakuda, A. Hayashi, and M. Tatsumisago: Preparation of amorphous Li<sub>4</sub>SiO<sub>4</sub>–Li<sub>3</sub>PO<sub>4</sub> thin films by pulsed laser deposition for all-solid-state lithium secondary batteries. *Solid State Ionics* **182**, 59 (2011).
- I. Seo and S.W. Martin: Fast lithium ion conducting solid state thin-film electrolytes based on lithium thio-germanate materials. *Acta Mater.* **59**, 1839 (2011).
- M. Yamashita and H. Yamanaka: Formation and ionic conductivity of Li<sub>2</sub>S–GeS<sub>2</sub>–Ga<sub>2</sub>S<sub>3</sub> glasses and thin films. *Solid State Ionics* **158**, 151 (2003).
- M. Tatsumisago, H. Morimoto, H. Yamashita, and T. Minami: Preparation of amorphous solid electrolytes in the system Li<sub>2</sub>S–SiS<sub>2</sub>–Li<sub>4</sub>SiO<sub>4</sub> by mechanical milling. *Solid State Ionics* **136–137**, 483 (2000).
- A. Hayashi, S. Hama, H. Morimoto, M. Tatsumisago, and T. Minami: Preparation of Li<sub>2</sub>S–P<sub>2</sub>S<sub>5</sub> amorphous solid electrolytes by mechanical milling. *J. Am. Ceram. Soc.* **84**, 477 (2001).
- J.E. Trevey, J.R. Gilsdorf, S.W. Miller, and S-H. Lee: Li<sub>2</sub>S–Li<sub>2</sub>O–P<sub>2</sub>S<sub>5</sub> solid electrolyte for all-solid-state lithium batteries. *Solid State Ionics* **214**, 25 (2012).
- J.E. Trevey, Y.S. Jung, and S-H. Lee: Preparation of Li<sub>2</sub>S–GeSe<sub>2</sub>–P<sub>2</sub>S<sub>5</sub> electrolytes by a single step ball milling for all-solid-state lithium secondary batteries. *J. Power Sources* **195**, 4984 (2010).
- M. Agostini, Y. Aihara, T. Yamada, B. Scrosati, and J. Hassoun: A lithium–sulfur battery using a solid, glass-type P<sub>2</sub>S<sub>5</sub>–Li<sub>2</sub>S electrolyte. *Solid State Ionics* **244**, 48 (2013).
- F. Mizuno, A. Hayashi, K. Tadanaga, and M. Tatsumisago: New, highly ion-conductive crystals precipitated from Li<sub>2</sub>S–P<sub>2</sub>S<sub>5</sub> glasses. *Adv. Mater.* **17**, 918 (2005).
- M. Tatsumisago and A. Hayashi: Superionic glasses and glass-ceramics in the Li<sub>2</sub>S–P<sub>2</sub>S<sub>5</sub> system for all-solid-state lithium secondary batteries. *Solid State Ionics* **225**, 342 (2012).
- K. Minami, A. Hayashi, S. Ujiie, and M. Tatsumisago: Electrical and electrochemical properties of glass–ceramic electrolytes in the systems Li<sub>2</sub>S–P<sub>2</sub>S<sub>5</sub>–P<sub>2</sub>S<sub>3</sub> and Li<sub>2</sub>S–P<sub>2</sub>S<sub>5</sub>–P<sub>2</sub>O<sub>5</sub>. *Solid State Ionics* **192**, 122 (2011).
- T. Ohtomo, A. Hayashi, M. Tatsumisago, and K. Kawamoto: Characteristics of the Li<sub>2</sub>O–Li<sub>2</sub>S–P<sub>2</sub>S<sub>5</sub> glasses synthesized by the two-step mechanical milling. *J. Non-Cryst. Solids* **364**, 57 (2013).
- A. Le Sauze and R. Marchand: Chemically durable nitrided phosphate glasses resulting from nitrogen/oxygen substitution within PO<sub>4</sub> tetrahedra. *J. Non-Cryst. Solids* **263–264**, 285 (2000).
- M.R. Reidmeyer and D.E. Day: Phosphorus oxynitride glasses. *J. Non-Cryst. Solids* **181**, 201 (1995).
- B. Wang, B.S. Kwak, B.C. Sales, and J.B. Bates: Ionic conductivities and structure of lithium phosphorus oxynitride glasses. *J. Non-Cryst. Solids* **183**, 297 (1995).

18. F. Muñoz, A. Durán, L. Pascual, L. Montagne, B. Revel, and A.C.M. Rodrigues: Increased electrical conductivity of LiPON glasses produced by ammonolysis. *Solid State Ionics* **179**, 574 (2008).
19. N. Mascaraque, J.L.G. Fierro, A. Durán, and F. Muñoz: An interpretation for the increase of ionic conductivity by nitrogen incorporation in LiPON oxynitride glasses. *Solid State Ionics* **233**, 73 (2013).
20. N. Mascaraque, H. Takebe, G. Tricot, J.L.G. Fierro, A. Durán, and F. Muñoz: Structure and electrical properties of a new thio-phosphorus oxynitride glass electrolyte. *J. Non-Cryst. Solids* **405**, 159 (2014).
21. F. Muñoz, L. Pascual, A. Durán, J. Rocherullé, and R. Marchand: Alkali and alkali-lead oxynitride phosphate glasses: A comparative structural study by NMR and XPS. *C. R. Chim.* **5**, 731 (2002).
22. C.D. Wagner, L.E. Davis, M.V. Zeller, J.A. Taylor, R.H. Raymond, and L.H. Gale: Empirical atomic sensitivity factors for quantitative analysis by electron spectroscopy for chemical analysis. *Surf. Interface Anal.* **3**, 211 (1981).
23. A. Hayashi, R. Araki, K. Tadanaga, M. Tatsumisago, and T. Minami: High resolution solid state NMR studies of ionically conductive  $\text{Li}_2\text{S}-\text{SiS}_2-\text{Li}_2\text{O}-\text{P}_2\text{O}_5$  oxysulphide glasses. *Phys. Chem. Glasses* **40**, 140 (1999).
24. K. Hirai, M. Tatsumisago, M. Takahashi, and T. Minami:  $^{29}\text{Si}$  and  $^{31}\text{P}$  MAS-NMR spectra of  $\text{Li}_2\text{S}-\text{SiS}_2-\text{Li}_3\text{PO}_4$  rapidly quenched glasses. *J. Am. Ceram. Soc.* **79**, 349 (1996).
25. K. Minami, F. Mizuno, A. Hayashi, and M. Tatsumisago: Structure and properties of the  $70\text{Li}_2\text{S}-(30-x)\text{P}_2\text{S}_5-x\text{P}_2\text{O}_5$  oxysulfide glasses and glass-ceramics. *J. Non-Cryst. Solids* **354**, 370 (2008).
26. R.K. Brow: Review: The structure of simple phosphate glasses. *J. Non-Cryst. Solids* **263–264**, 1 (2000).
27. B.C. Bunker, D.R. Tallant, C.A. Balfe, R.J. Kirkpatrick, G.L. Turner, and M.R. Reidmeyer: Structure of phosphorus oxynitride glasses. *J. Am. Ceram. Soc.* **70**, 675 (1987).
28. A. Le Sauze, L. Montagne, G. Palavit, F. Fayon, and R. Marchand: X-ray photoelectron spectroscopy and nuclear magnetic resonance structural study of phosphorus oxynitride glasses, ‘LiNaPON’. *J. Non-Cryst. Solids* **263–264**, 139 (2000).
29. S. Veprek, S. Iqbal, L.J. Brunner, and M. Scharli: Preparation and properties of amorphous phosphorus nitride prepared in a low-pressure plasma. *Philos. Mag.* **43**, 527 (1981).
30. R. Marchand, D. Agliz, L. Boukbir, and A. Quemerais: Characterization of nitrogen containing phosphate glasses by X-ray photoelectron spectroscopy. *J. Non-Cryst. Solids* **103**, 35 (1988).
31. R.K. Brow, M.R. Reidmeyer, and D.E. Day: Oxygen bonding in nitrided sodium- and lithium-metaphosphate glasses. *J. Non-Cryst. Solids* **99**, 178 (1988).
32. R. Brückner, H-U. Chun, H. Goretzki, and M. Sammet: XPS measurements and structural aspects of silicate and phosphate glasses. *J. Non-Cryst. Solids* **42**, 49 (1980).
33. D. Foix, D. Gonbeau, G. Taillades, A. Pradel, and M. Ribes: The structure of ionically conductive chalcogenide glasses: A combined NMR, XPS and ab initio calculation study. *Solid State Ionics* **3**, 235 (2001).